González Benito, Javier; Torres, Diego; Ballesteros, Carmen; Ruiz, Víctor M.; Teno, Jorge (2019) PVDF based nanocomposites produced by solution blow spinning, structure and morphology induced by the presence of MWCNT and their consequences on some properties. *Colloid and Polymer Science*, 297(7-8), pp.: 1105–1118.

DOI: https://doi.org/10.1007/s00396-019-04530-5

PVDF Based Nanocomposites Produced by Solution Blow Spinning, Structure and Morphology Induced by the Presence of MWCNT and their Consequences on Some Properties

Javier González-Benito,[1*] Diego Torres,[1] Carmen Ballesteros[2], Victor M. Ruiz[1] and Jorge Teno[1]

[1]Dept. Materials Science and Engineering, IQMAAB. Universidad Carlos III de Madrid, Av. Universidad 30, 28911 Leganés (Madrid), Spain.
[2]Dept. of Physics, Universidad Carlos III de Madrid, Avenida de la Universidad 30, 28911 Leganés (Madrid), Spain.

[*]Corresponding author
Address: Av. Universidad 30, 28911 Leganés (Madrid – Spain)
Phone: +34 916248870
Fax: +34 916249430
e-mail: javid@ing.uc3m.es
ORCID iD: 0000-0002-8864-0971

Acknowledgements

The authors appreciate the financial support received from the Ministerio de Economía y Competitividad [MAT2014-59116-C2]; the Universidad Carlos III de Madrid due to Fondos de Investigación de Fco. Javier González Benito [2012/00130/004] and the strategic Action in Composites materials and interphases [2011/00287/002]. TEM characterization was made at LABMET, associated to the Red de Laboratorios de la Comunidad de Madrid.

Abstract

Nanocomposites based on poly(vinylidene fluoride), PVDF, filled with multiwalled carbon nanotubes, MWCNT were prepared by solution blow spinning, SBS. PVDF was modified with MWCNT with the aim of changing final properties inducing structural and morphological variations in the polymer by the simple presence of conductive particles. Different compositions were considered (0%, 1%, 2%, 3% and 5% by weight of MWCNT) to understand the influence of the presence of MWCNT on the polymer structure, morphology and consequently other properties. Morphology was inspected by optical and electron (SEM and TEM) microscopies, while structure was studied by Fourier transformed infrared spectroscopy, FTIR. Thermal behavior was monitored by differential scanning calorimetry, DSC, while the surface and electrical properties were studied by contact angle and capacitance measurements respectively. SBS allowed obtaining mats of nanocomposites constituted by submicrometric fibers where the MWCNT are uniformly dispersed and well aligned along the PVDF fibers. In this study several aspects about structure and thermal behavior of PVDF were clarified in relation to other researches carried out up to the moment. Although MWCNT concentration did not seem to affect much the fibrous morphology of the SBS materials, the PVDF crystalline structure and surface properties of the materials were slightly modified. Dielectric behavior of PVDF was highly affected by the presence of MWCNT leading to a particular change in the permittivity and being possible to obtain a value of 0.023 for the percolation fraction.

Keywords: Carbon nanotubes; nanofibers; Poly(vinylidene fluoride); Solution blow spinning.

1. Introduction

Recently, one of the great challenges of many scientists and engineers is to develop smart textiles for clothing. Among other characteristics, they should be ultralight, flexible, superhydrophobic and easily processable materials with some especial properties that usually are ascribed to metals and/or ceramics such as, high electric conductivity or permittivity, etc. Although polymers have low density and are easily processed, only a few of them gather other properties like those above mentioned. A common way to overcome these technological needs claimed by the society is to look for the best combination between different materials with the aim of finding new synergistic effects that only can be explained by physico-chemical reasoning.

Several researchers suggest that filling polymers with conductive particles is an easy way to tune properties, for example, from materials of low permittivity to materials with high dielectric constant or even, to electrical conducting materials. When adding the conductive particles it is expected to be formed small capacitors within the polymer (the dielectric). Assuming the previous hypothesis, a high amount of particles added should lead to many capacitors what should allow increasing the electrical permittivity, at least, until the percolation fraction is reached. When enough conductive particles are added as to create conductive paths through which electrons can be moved by the action of an electric field percolation has been reached. In fact, some works already shown how the electrical permittivity of polymers increases adding conductive particles near the percolation fraction [1–7]. In those cases, it is reasonable to think that the presence of multiple micro- or even nano-capacitors must be the cause of such capacitance increase. In fact, the main contributing factors are the available surface area of the electrodes (conductive particles) and the thickness of the dielectric (the polymer) because capacitance is directly proportional to the surface area of contact and inversely proportional to the thickness of the dielectric. Therefore, the amount of conductive nanoparticles should play a very important role on the electrical properties of the nanocomposites since, the higher number of particles the larger the surface of contact between the conductors and the dielectric and, in addition, the thinner the layer of dielectric.

On the other hand, the shape (aspect ratio), size and the dispersion of nanoparticles within a polymer matrix should also contribute to the electrical behavior of nanocomposites. For example, it seems reasonable to think that particles in the form of nanoplatelets (graphene for instance) are the best fillers to achieve those small capacitors within the polymer matrix, after them nanofibres and nanotubes (carbon nanotubes) and finally, other kind of particles with different shapes. Besides, dispersion must be also an important factor since uniform dispersion should ensure the maximum efficiency in terms of space occupation and therefore available filler surface to be in contact with the polymer. In the case of platelets, fibers and tubes it is evident that a parallel arrangement of them without forming aggregates should lead to the optimal dispersion of particles. Therefore, methods to disperse particles that favor a parallel arrangement of them are preferred.

Carbon nanotubes, single (CNT) or multiwalled (MWCNT), can be a good choice to enhance the permittivity of polymers by the preparation of nanocomposites because of their high electrical and thermal conductivities. Besides, due to their aspect ratio CNT should facilitate the formation of conducting channels, leading to quite low percolation

thresholds. Other interesting characteristics of CNT are their high tensile strength and Young's modulus with values around 100 GPa and 500 GPa, respectively [8] , which make them good candidates to improve mechanical properties of polymers [9, 10].

Among the polymers with especial electrical properties, poly(vinylidene fluoride), PVDF, is receiving special attention [11]. It is a semicrystalline polymer with piezo and pyroelectric properties. This polymer is biocompatible, presents good mechanical strength and is quite resistant against hydrolysis, abrasion and radiation [12]; therefore, its choice respect to other conventional electroactive materials can be easily justified. However, properties of PVDF based materials are highly dependent on the morphology and polymer structure.

One of the most interesting peculiarities of PVDF is that it may mainly appear in four different crystalline phases, α, β, γ and δ or mixtures of them [13–15]. The most stable is the α phase; however, the β phase is the most popular because it presents the highest piezo- and pyroelectric responses [16, 17]. Thus, important efforts have been addressed to increase the fraction of β phase, trying to improve the electroactive behavior of the polymer. Regarding this issue, reported literature points out that, in general, the main methods to increase the β phase fraction in PVDF are: i) preparation of films from solution after a controlled process of evaporation [18–20] and ii) to induce conformational changes on the polymeric chains by exerting certain stresses that enhance the preferential orientation of the macromolecules [10, 21–23].

On the other hand, it has been also shown that the addition of certain fillers within semicrystalline polymers may affect, among others, the morphology in terms of spherulites and lamellar sizes, and the crystalline structure [15, 18, 24–27]. In fact, it was reported that addition of CNT to PVDF can induce appearance of β-phase [10, 28]. Besides, carbon nanotubes may act as nucleating agents of PVDF exerting a crystallization confinement that depends on the nanotubes concentration [29, 30]. Therefore, if carbon nanotubes are dispersed in a parallel way within PVDF polymer, by simply changing the composition, nanocomposites covering a wide range of electrical properties should be able to obtain. However, to overcome the later, it would be necessary to look for a processing method that allows obtaining a uniform dispersion of nanoparticles that, in addition, helps to orient the macromolecular chains.

Among the existing processing methods, electrospinning, ES [31] and solution blow spinning, SBS [32, 33] might be good candidates. Several authors have demonstrated that fibrous composites formed by carbon nanotubes dispersed in polymers can be fabricated by electrospinning, being the carbon nanotubes well aligned within the polymeric fibers [34–36]. However, this method of processing needs to apply high voltages between the polymer dispenser and a conductive target where the fibers are deposited. Besides, this method usually implies low deposition rates so, for certain applications it can be a disadvantage in terms of mass production. In those cases, SBS seems to be a better option. It allows direct dispensation of mat films onto specific locations or substrates with a considerable higher material production rate [32, 37, 38]. After finding the best conditions, SBS may produce micro and submicrometric fibers similar to those obtained by electrospinning [32, 33]. The process is carried out with a device composed by a concentric nozzle through which a polymer solution is ejected by the action of pressurized gas also introduced in the nozzle. Besides, as far as the present

authors know there are not many works published about mats of submicrometric fibers created by SBS where carbon nanotubes are dispersed in a polymer [39].

In this work, PVDF based nanocomposites in the form of mats are fabricated by SBS. Multiwalled carbon nanotubes are used as the nanofiller. Apart from this, different amounts of MWCNT or nocomposite composition are taking into consideration. On the other hand, physico-chemical characterization of the obtained materials is carried out in order to understand the influence of the presence of carbon nanotubes on the PVDF structure and morphology so as their direct and/or indirect effect in some of the final properties of the composites.

2. Materials and Methods

2.1. Materials

To prepare the nanocomposites poly(vinylidene fluoride), PVDF, was used as the polymer matrix (Sigma-Aldrich; Mn = 10,700; Mw = 27,500; and density 1.78 g/cm^3) and multi-walled carbon nanotubes, MWCNT, as the nanofiller (Sigma-Aldrich; with 95 wt% of pure carbon, diameters ranging from 6 to 9 nm, lengths of about 5 μm and density 2.1 g/cm^3). Dimethylformamide, DMF, and acetone, Ac, HPLC grade solvents (Aldrich) were used to prepare the solutions and suspensions to be blow spun.

2.2. Samples preparation

A mixture of DMF/Ac with a volume ratio of 1:9 was used as the solvent to prepare the solutions and suspensions for the SBS process. Then, the mount of polymer necessary was added to the solvent to finally have mixtures of 11% by weight in terms of PVDF. On the other hand, to prepare the suspensions, the required amount of MWCNT were firstly added to 4 mL of the DMF/Ac mixture, sonicated for 30 min at room temperature and finally added to the PVDF solution in DMF/Ac. The relative amounts of MWCNT in the composites considered in the present work were 0%, 0.5%, 1%, 2%, 3% and 5% by weight respectively.

Films in the form of mats of PVDF based materials were obtained using a home-made SBS equipment inspired in that patented by Medeiros et al. [32, 40] The SBS machine is composed by a nozzle connected to an air compressor with a pressure regulator and a plastic syringe coupled to an automatic pump (NE 1000 X, New Era System, Inc., Farmingdale, NY). The nozzle was made of a tube (inner diameter 0.7 mm) of aluminum with a hole to introduce air at 2 bars, and a glass capillary (inner diameter 0.5 mm) positioned along the aluminum cylinder so it protruded 2 mm beyond. The mixtures pumped at 0.5 mL/min and ejected from the nozzle were deposited on a rotating cylindrical collector wrapped with aluminum foil (Fig. 1) and located at 15 cm of working distance.

Fig. 1 Mat of PVDF/MWCNT material deposited on a cylindrical collector.

2.3. Equipments

Sample thicknesses were measured using a thickness-meter Easy-check FN of NEURTEK Instruments with an accuracy of ± 1 μm and a Digimatic micrometer (Mitutoyo Corporation) with also an accuracy of ± 1 μm. Six measurements were performed with each micrometer and, finally, the mean value from the 12 measurements was taken.

The morphology of the samples was studied by optical, OM, and scanning electron, SEM, microsocopies. In the first case, an opto-digital microscope OLYMPUS DSX500 was used to obtained 3D images (objective ×40). Twenty linear profiles were taken from the 3D images to subsequently extract roughness parameters. In the second case, submicrometric fibers were inspected with a Philips XL30 scanning electron microscope, using the secondary electrons signal, SE. To avoid charge accumulation, samples were gold coated by sputtering with a conventional anodic deposition method using a low vacuum coater Leica EM ACE200.

To see the MWCNT within the PVDF, transmission electron microscopy, TEM, was used (Philips Tecnai 20F FEG analytical microscope operating at 200 kV).

Viscosity measurements were carried out using a Haake viscosimeter iQ Rheometer (Thermo Scientific) at 20 ºC and in a parallel plane configuration (Plate P60/Ti/SE). Nine cycles ranging from 100 to 900 s^{-1} were performed taking 100 measurements during each cycle in 30 s.

Infrared spectroscopy was performed in the transmission mode using a FT-IR Spectrum GX (Perkin-Elmer). As transparent sample holder to IR radiation, potassium bromide (KBr) discs were used. Systems to be studied were simply blow spun on the KBr discs. Spectra were recorded in the range 400-4000 cm^{-1} taking the average of 20 scans with a resolution of 2 cm^{-1}.

Thermal analyses were carried out by differential scanning calorimetry, DSC, using a Mettler Toledo 822e calorimeter under nitrogen atmosphere. Samples (2-4 mg) were subjected to four thermal cycles: i) a heating process from 30 to 190 ºC at 10 ºC/min; ii)

an isothermal process at 190 ºC for 10 minutes to ensure that the processing and thermal history of the samples are erased; iii) a cooling process from 190 ºC to 30 ºC at 10 ºC/min and iv) a second heating from 30 to 190 ºC at 10 ºC/min. The melting points, Tm, and the enthalpies of fusion, ΔH_m, were obtained from the DSC endothermic peaks and their integrations respectively. To calculate the crystallization degree, X_c, the following equation was used (eq. 1).

$$X_c = \frac{\Delta H_m}{(1-x)\cdot \Delta H_m^0} \qquad (1)$$

where x is the weight fraction of MWCNT and ΔH^o_m is the standard enthalpy of fusion for the fully crystallized PVDF, ΔH^o_m = 104.7 J/g [41]. It is important to highlight that apart from knowing the influence of the presence of the MWCNT on the thermal behavior it is also important to study the influence of the processing method used (the solution blow spinning). That was the reason way the DSC trace of the first heating was analyzed without erasing the thermal and/or processing history of the materials.

Surface characteristics of the materials were studied by contact angle measurements using an OCA-15 KRÜSS GmbH tensiometer based on the drop method. Distilled and deionized water was used as the test liquid. The final value of contact angle was taken from the average of the contact angles measured from 10 drops of 3 μL deposited on different locations of the same surface.

The electrical tests were carried out using a homemade cell composed of two aluminum circular electrodes with a stem supported by a structure made of two thick sheets of poly methyl methacrylate (see Fig. 2). Circular specimens were located in between the circular electrodes (12 mm of diameter) while the cell was connected to the equipment of measurement through copper wires. After making a slight pressure with a couple of wing nuts, the capacitance, C, of the samples was directly measured using a digital multimeter Mod 60.131 ELECTRO DH. The dielectric constant (k) or relative permittivity, ε_r, was calculated from the expression:

$$\varepsilon_r = \frac{d}{A\cdot \varepsilon_o} \cdot C \qquad (2)$$

where ε_0 = 8.854 $\times 10^{-12}$ F/m is the permittivity of vacuum, A, the electrode area in contact with the sample and d the thickness of the sample.

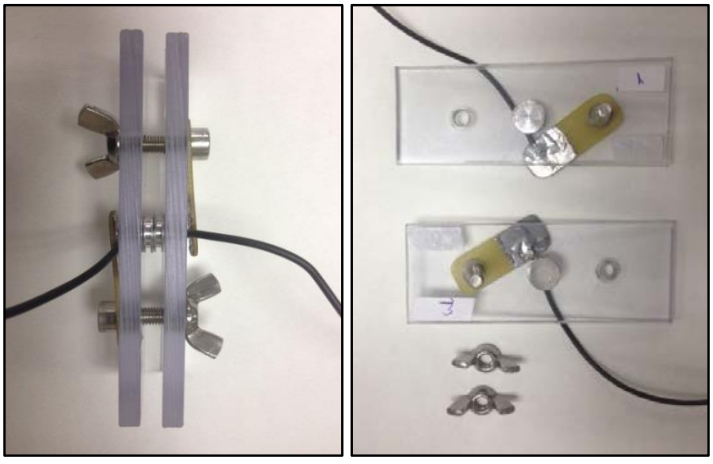

Fig. 2 Home-made cell to carry out the electrical tests.

3. Results and Discussion

In Fig. 3, as an example, plane projections of 3D optical images of PVDF with and without MWCNT are presented. For all the samples, the morphology consisted on webs made of fibers sometimes interconnected by lumps of material. The materials with MWCNT showed dark regions, pointing out accumulation of MWCNT as expected attending their opacity. After a more careful observation it can be seen how dark spots are distributed all along the fibers (see zoomed image in Fig. 3c) which suggests a quite good dispersion of the MWCNT throughout the fibers. However, the optical images had not resolution enough as to give the dimensions of the fibers and, therefore, to fully study the influence of the presence of the MWCNT on the final morphology of the materials. Besides, optical microscopy observations do not offer the possibility of accurately locating the MWCNT within the PVDF. Due to this, nanocomposites were inspected by TEM.

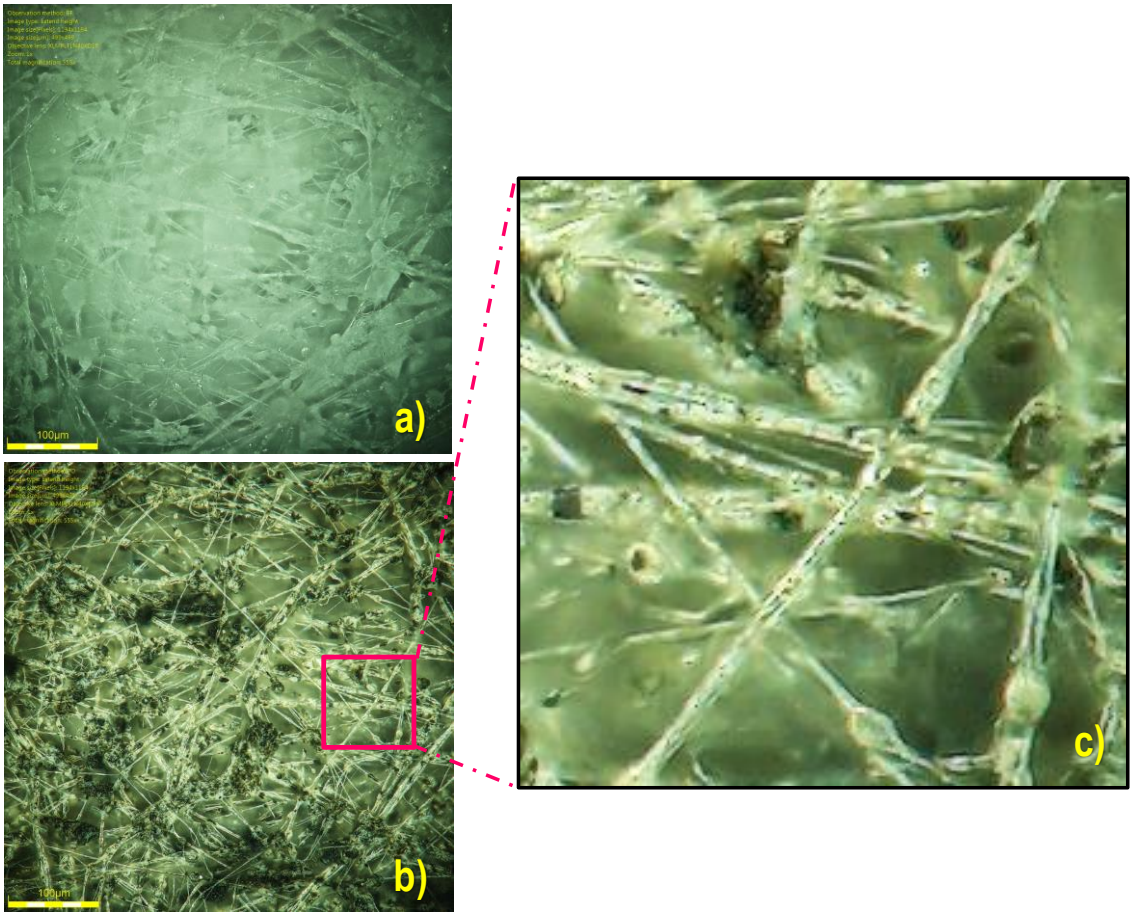

Fig. 3 Plane projection of 3D optical images of a) PVDF; b) PVDF 1% MWCNT by weight and c) zoomed area of image b). Scale bars indicate 100 µm.

In Fig.4 a representative TEM image of SBS fibers of the nanocomposite with 1% wt of MWCNT is shown. Two fibers with diameters of 110 nm and 450 nm respectively and

a region with more accumulation of material are shown. It can be highlighted two regions represented as zoomed images (500 nm of size) in Fig. 4. The region A, showing how the nanotubes are mainly placed stretched along the SBS fiber and, the region B which would represent one of those lumps of material shown in the optical images (Fig. 3), where the nanotubes seem to be arranged in a random coil way. Although it seems that the random coil arrangement of MWCNT in the region B occurs within a kind of PVDF globules, SEM images, as will be seen later, shown that those globules are actually formed by thin fibers. This result suggests that MWCNT are always arranged throughout the polymer fibers; in other words, SBS, under the conditions selected, allows obtaining a good alignment of MWCNT within the PVDF fibers and, therefore, achieving one of the most important prerequisites for an effective reinforcement if the load is applied parallel to the nanofiller arrangement.

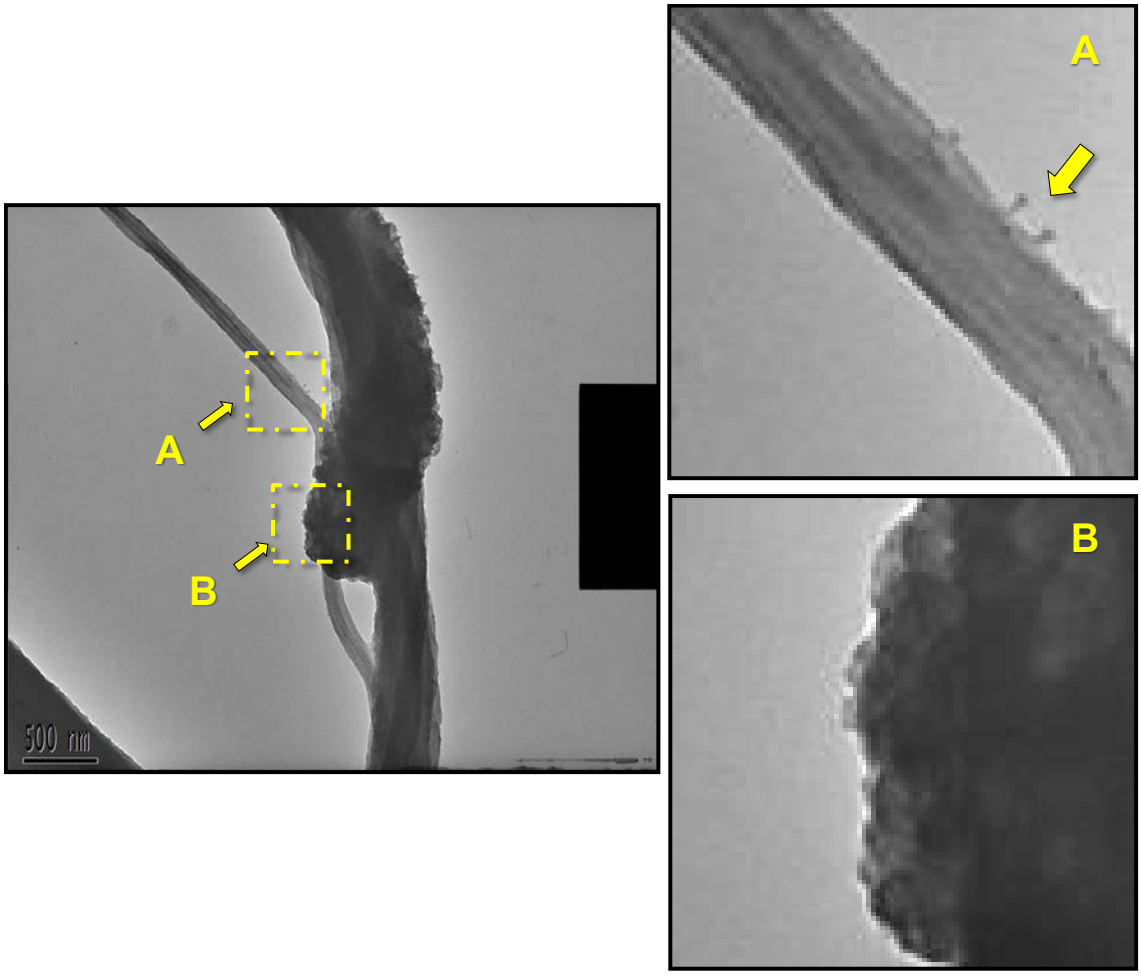

Fig. 4 TEM image of representative SBS fibers obtained for the nanocomposite with 1% wt of MWCNT. Scale bar indicates 500 nm.

In Fig. 5 and 6 SEM images of blow spun nanocomposites with different amount of MWCNT are presented. In every case fibrous morphology was observed. In general, the mean diameter of the fibers does not seem to change with the amount the MWCNT added to the PVDF polymer. However, if there were any particular tendency in the fibers sizes it should be better seen in the histograms shown as insets in Fig. 5. From these histograms the standard deviation, σ, the first moment of the distributions, $\langle D \rangle$,

the most probable diameter, D_m, so as the data dispersion represented by the quotient between the second and the first moment of the distribution, Γ, can be obtained (Table 1).

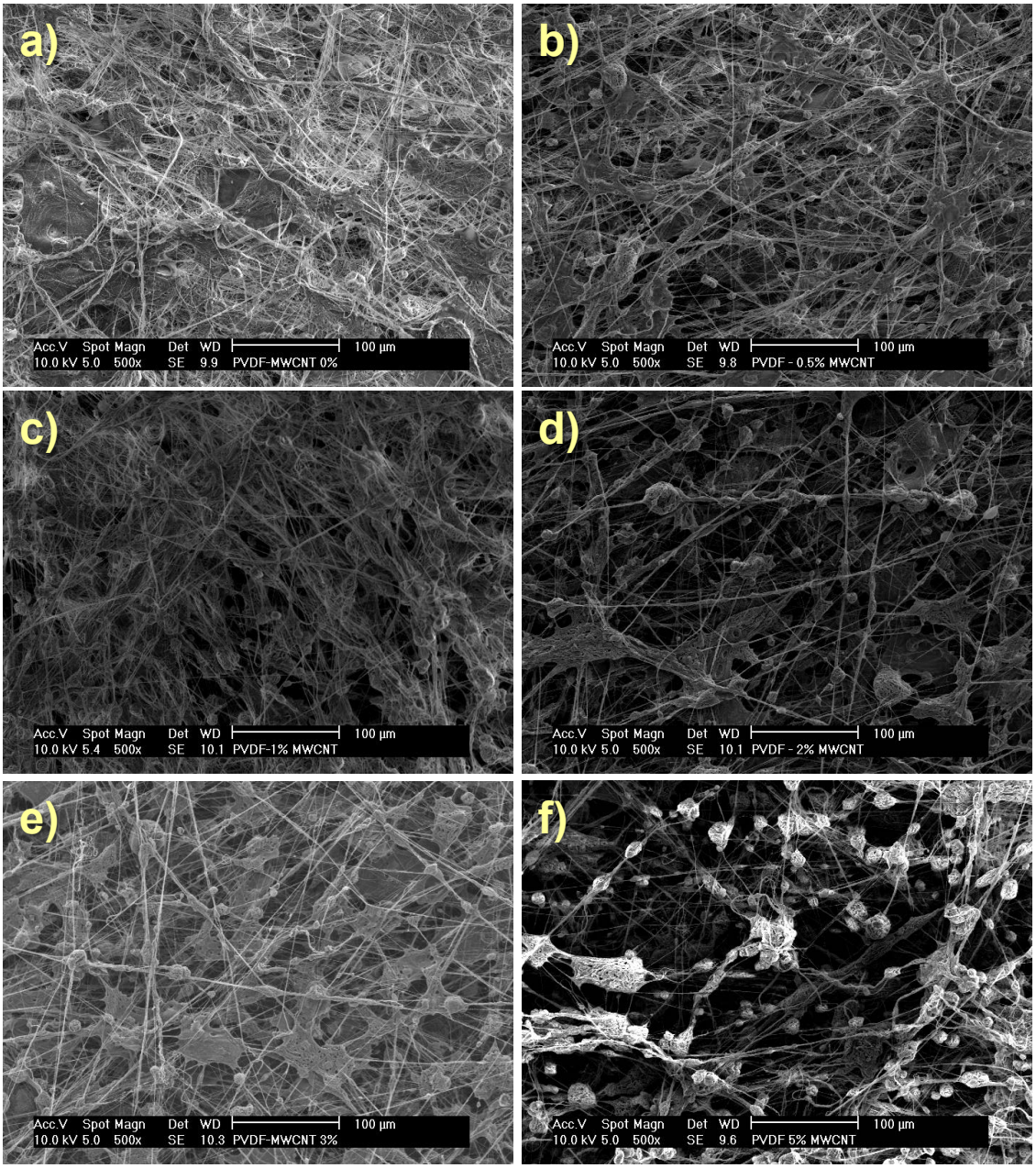

Fig. 5 SEM images of solution blow spun nanocomposites with different amount of MWCNT (weight percentages): a) 0%; b) 0.5%; c) 1%; d) 2%; e) 3% and f) 5%.

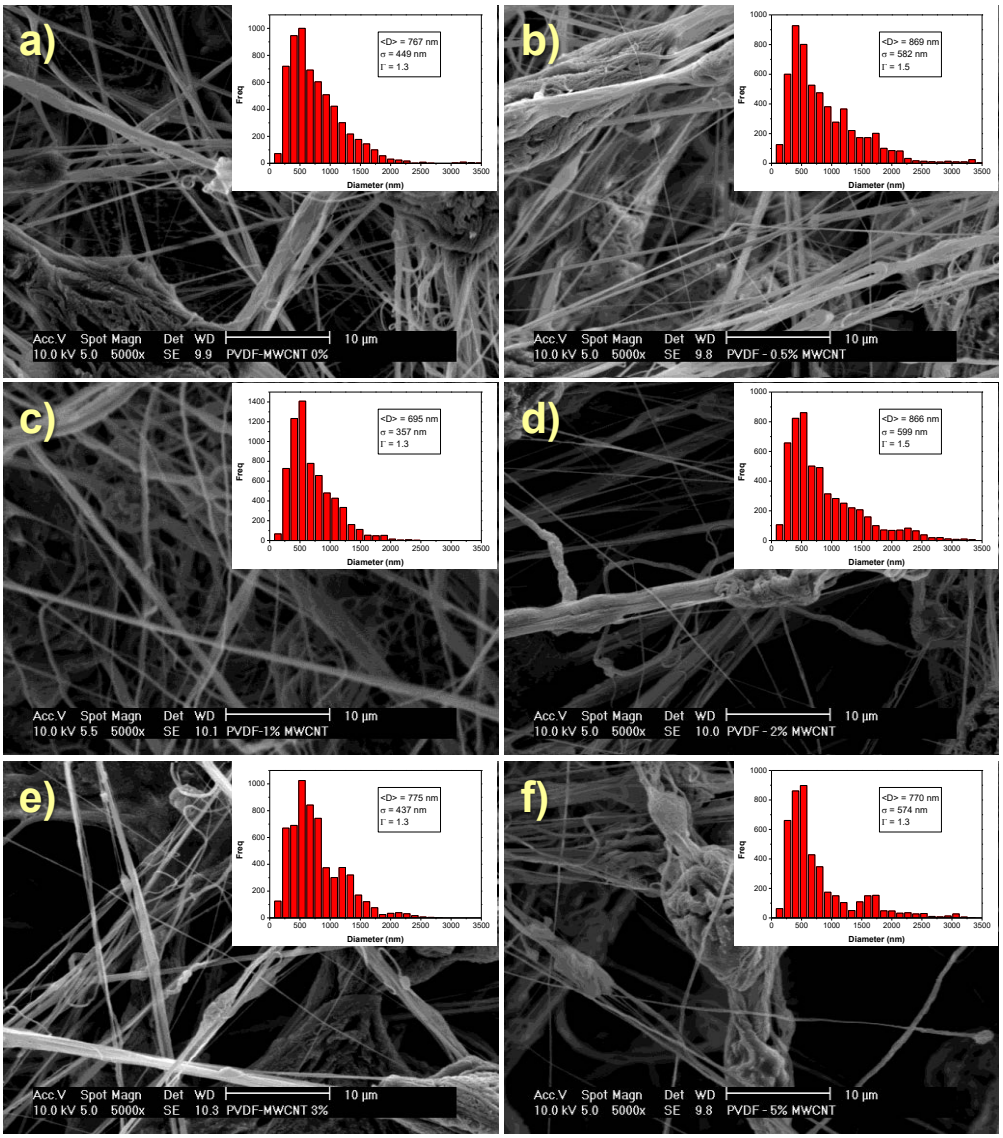

Fig. 6 SEM images of solution blow spun nanocomposites at different amount of MWCNT (weight percentages): a) 0%; b) 0.5%; c) 1%; d) 2%; e) 3% and f) 5%.

As can be seen, correlations cannot be found between the fibers morphology and the amount of MWCNT. There is only one difference observed as a function of nanofiller content, the amount of fibers caking in the form of globules, in agreement with that observed by optical microscopy. By a careful observation of one of those globules it can be concluded that they are mainly formed by an accumulation of fibers (Fig. 6). Seoul et al. fabricated similar materials by electrospinning. They shown a clear dependence of the viscosity and other properties of the suspensions on the nanofiller content represented by changes in the morphology [42]. Therefore, one might think that viscosity changes is one of the main causes affecting solution blow spun fibers. In fact, Fig. 7 shows how there is a clear viscosity increase of the MWCNT suspensions as the MWCNT amount increases.

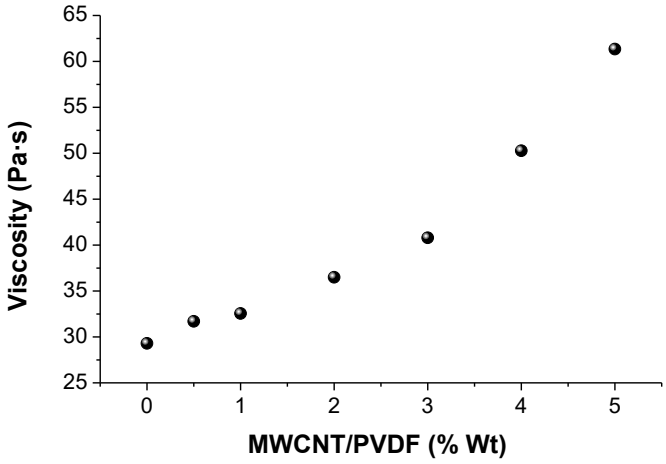

Fig. 7 Viscosity of MWCNT suspensions as a function of the relative amount of MWCNT respect to PVDF.

Table 1 Statistical parameters obtained from the histograms of Fig. 5: Standard deviation, σ, the first moment of the distributions, <D>, the most probable diameter, Dm, and data dispersion, Γ.

Sample	MWCNT (% wt)	<D> (nm)	D_m (nm)	σ (nm)	Γ
PVDF-0%	0	767	408	449	1.3
PVDF-0.5%	0.5	869	392	582	1.5
PVDF-1.0%	1	695	413	357	1.3
PVDF-2.0%	2	866	405	599	1.5
PVDF-3.0%	3	775	475	437	1.3
PVDF-5.0%	5	770	396	574	1.3

It is evident that for SBS, as in the case of electrospinning, changes in the viscosity of the suspension should lead to differences in its output speed from the nozzle. For higher viscosity, slower displacement of the suspension is expected, favoring higher accumulation of material in the nozzle gate. Besides, higher viscosities should exert more resistance to the deformation of the suspension. Both consequences of higher viscosities suggest the creation of thicker fibers by solvent evaporation.

However, more factors affecting the fiber formation during their time of flight are expected; among them, one of the most important seems to be the evaporation rate, which, in turn, depends on many other factors such as room conditions (temperature, pressure, and relative humidity), nature of the components and composition of the suspension. Therefore, a conclusive analysis of the morphology of the SBS materials with physico-chemical meaning would require an especial work only focused to this particular issue.

In Fig. 8 FTIR spectra of the SBS samples are represented. Well documented bibliography about the bands assignment respect to the main phases appearing in the PVDF were used [15, 43]. Dotted lines were drawn in Fig. 8 pointing out the position

where the characteristics bands of the main polymorphs should appear. After this, the method proposed by Cai et al [43] was followed to quantify the presence of the three main phases and to study the influence of the incorporation of MWCNT.

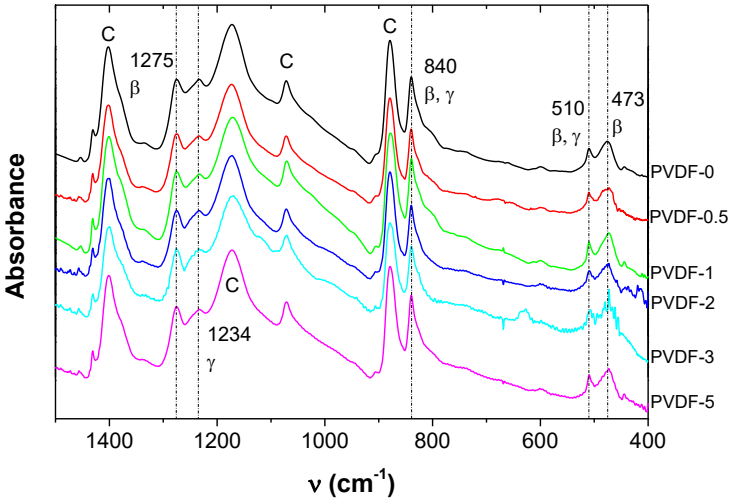

Fig. 8 FTIR spectra of all the SBS samples prepared.

First of all, the peaks considered as common peaks (880, 1072 and 1401 cm^{-1}) were taken out from the analysis because they might belong to any of the three main phases [43]. As can be seen at 614 cm^{-1} and 763 cm^{-1}, where usually appear two of the sharpest bands of α phase, there is not any peak. This result points out that solution blow spinning of the system PVDF/MWCNT, at least under the processing conditions used, leads to materials for which the PVDF does not crystallize in the α phase. On the other hand, the exclusive bands of the β phase at 473 and 1275 cm^{-1} and the exclusive band of the γ phase at 1234 cm^{-1} could be identified (Fig. 8), suggesting that both phases of the PVDF appear in the materials under study. Taking into account the experimental evidences already mentioned, it is clear that one way of quantifying the relative amount of β and γ phases would be the use of the relative absorbances (peak area or peak height) of the two bands at 1275 and 1234 cm^{-1} respectively as proposed Cai et al [43]. Although in the present work the same idea for the analysis was taken, the analytical expression was slightly changed.

Instead of using height differences between peaks and the nearest valleys, the absolutes absorbances were taken after a base line correction between the minima [44, 45].

$$F(\beta) = F_{EA} \times \left(\frac{A_\beta}{A_\beta + A_\gamma}\right) \qquad (3)$$

where F(β) is the fraction of β phase, FEA is relative fraction of the electroactive phases β and γ that should have a value of 1 since no evidence of α phase was observed in the FTIR spectra (Fig. 8). A_β and A_γ are the absolute absorbances at 1275 cm^{-1} and 1234 cm^{-1} respectively after the corresponding base line correction.

In Fig. 9 the relative amount of β phase is represented as a function of the MWCNT content. It is observed a slight tendency of β phase to increase when carbon nanotubes

are added to the PVDF by solution blow spinning. This result is in accordance with those obtained by other researchers for PVDF composites using different nanomaterials, e.g. clay, metal, metal oxide nanoparticles, CNTs and grapheme. In those cases, it was stated that nanofillers favor the formation of piezoelectric polymorphs [46–48].

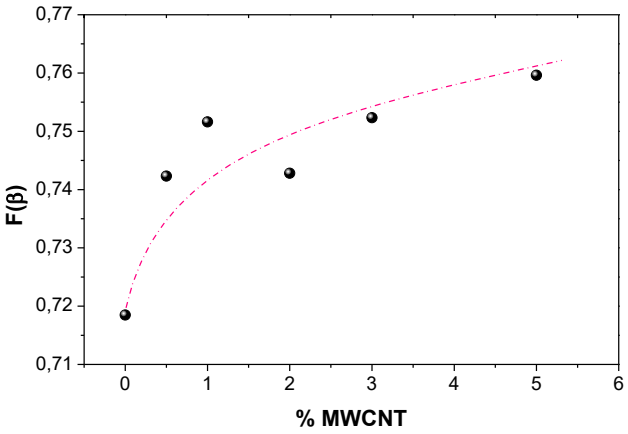

Fig. 9 Relative amount of the β phase plotted as a function of the MWCNT content.

In Fig. 10a DSC traces corresponding to the first heating of all the samples under study are shown. Typical endothermic peaks at 165 ºC are obtained. They can be ascribed to the PVDF melting process. Although it can be seen small differences in the general profile of the endotherms they do not seem to be due to changes in the MWCNT content since correlations were not observed. A possible explanation of those slight variations might be due to motions in the spun fibers when the melting process is occurring.

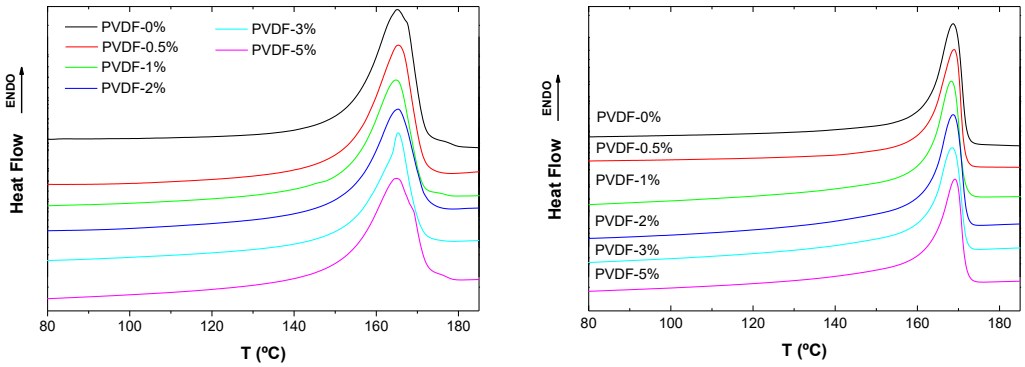

Fig. 10 DSC traces corresponding to the first (a) and second (b) heating scans of all the samples under study.

Considering data elsewhere published about the melting temperature of PVDF obtained from DSC thermograms there is an important discrepancy about the interpretation of the values taken at the maxima of the endothermic peaks [15, 46, 48–54].

In general, lower values of melting temperatures, at about 165 ºC, are usually assigned to the fusion of the α phase [46, 48, 49, 53]; however, this assignment would not be in

accordance with our results since FTIR clearly showed the presence of mainly β phase in the samples under study (with endothermic peaks at 165 ºC, Fig. 9a). However, while some authors have stated the opposite [55] respect to the assignation of the polymorphs from the DSC results, other affirmed that the DSC only allows evaluating with accuracy the degree of crystallinity of PVDF and it does not seem to be very useful for distinguishing between the different phases, at least between α and β phases since the melting temperatures of these polymorphs are very close, both appear in the range 162–172 ºC [56].

Only in the case of the γ phase the DSC seems to differentiate it from the other polymorphs since its melting peak is observed at higher enough temperatures in the range 179–180 ºC [57, 58]. Therefore, the most plausible explanation for the shifts observed in the melting temperatures found in the range 160-172 ºC is to consider that they are more likely to be due to differences in the lamella thicknesses and other morphologic variations rather than by the difference in the proportion of crystalline phases [52, 59]. An experimental evidence of the later are the results obtained in the second DSC heating scans (Fig. 10b), after erasing the thermal history. In those cases, regardless the MWCNT content, all melting peaks appear at higher temperatures close to 169 ºC.

In fact, after erasing the thermal history the α phase is the main polymorph in the samples as can be deduced from the FTIR spectra (Fig. 11) which clearly show bands at 614 cm^{-1} and 763 cm^{-1} respectively. Therefore, higher melting temperatures does not necessarily mean higher content of β phase.

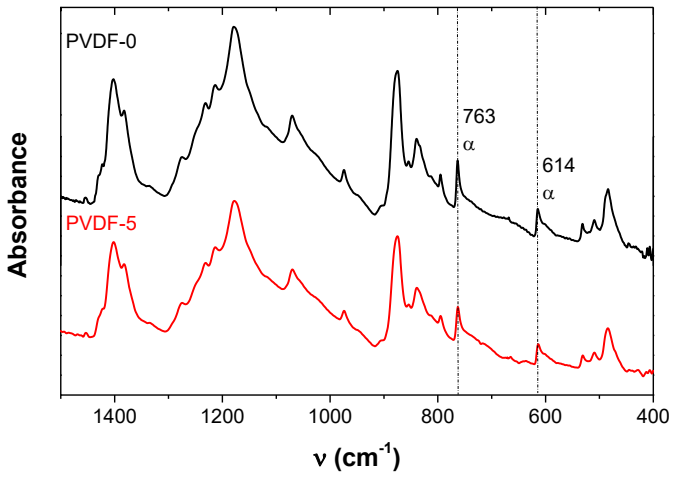

Fig. 11 FTIR spectra of neat PVDF and PVDF filled with 5% of MWCNT, in both cases after erasing the thermal history.

Assuming the absence of the α phase for the SBS samples one way of estimating the value of the melting temperature for the β phase, T_β, may be the use of a simple rule of mixtures taking the quite accepted value of 180 ºC for the melting temperature of the γ phase, T_γ [57, 58].

$$Ts = F(\beta)\cdot T_\beta + [1-F(\beta)]\cdot T_\gamma \qquad (4)$$

where T_s is the melting temperature of the sample and F(β) is the volume fraction of the β phase.

Therefore:

$$T_\beta = \frac{T_S - [1 - F(\beta)] \cdot T_\gamma}{F(\beta)} \qquad (5)$$

Taking the values from the Fig. 9, a value of 160 ± 1 ºC was obtained for the melting point of the β phase. On the other hand, for the first heating scans the average of the melting temperatures taken at the maxima is 165 ºC with only a deviation of ±1 ºC. This result suggests that in the case of occurring any phase variation as a function of the nanofiller content, it should be so low as to lead to the thermal changes to be within the thermal accuracy of the DSC, ± 0.5 ºC. Using the melting temperatures of 160 ºC and 180 ºC for the beta and gamma phases respectively, taking again the FTIR results (Fig. 9) and taking into account that the crystalline fraction obtained from eq (1) remains constant regardless the filler content with a value of about 51 ± 4 %, the highest variation expected on the melting temperature would be of only 0.8 ºC close to the DSC accuracy.

The Table 2 gathers the average values of the roughness parameter R_a and the contact angle with water for some of the samples prepared (representative images of water drops used to measure the contact angles on the materials under study are shown in Figure 12). Considering the error, the roughness does not change with the filler content which will be in accordance with the morphology results obtained from the analyses of the SEM images (Table 1). However, the values of roughness seem to reflect certain tendency. There is a slight roughness increase when the amount of MWCNT increases in the nanocomposites. On the other hand, the contact angle formed by a drop of water follows the same tendency suggesting that the addition of MWCNT to the PVDF by SBS increases the hydrophobicity of the materials due to the simply increase of roughness. This result may have interesting consequences in terms of the final application of this kind of materials; for instance, when they have to be used in adverse ambient conditions where the presence of water could cause serious damages.

Table 2 Average values of the roughness parameters R_a, R_q and the contact angle with water.

Sample	MWCNT (% wt)	R_a (μm)	R_q (μm)	CA (º)
PVDF-0%	0	2.1 ± 0,5	2.7 ± 0.6	129 ± 4
PVDF-0.5%	0.5	2.0 ± 0.3	2.5 ± 0.3	132 ± 2
PVDF-1.0%	1	2.3 ± 0.4	2.9 ± 0.5	132 ± 4
PVDF-2.0%	2	2.5 ± 0.4	3.1 ± 0.5	134 ± 4
PVDF-3.0%	3	2.1 ± 0.5	2.6 ± 0.6	134 ± 3
PVDF-5.0%	5	2.8 ± 0.7	3.4 ± 0.9	136 ± 6

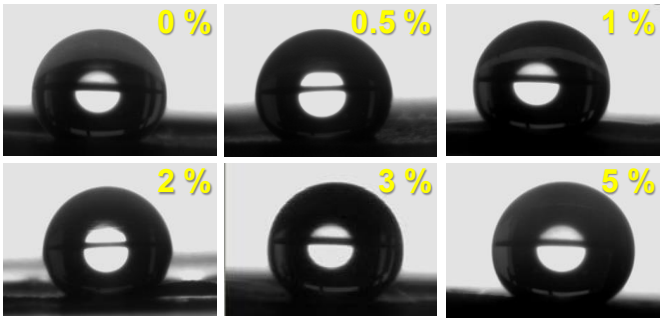

Fig. 12 Representative images of water drops used to measure the contact angles on the materials under study. Compositions in weight percent of MWCNT are written on the images.

In the Table 3 the averaged values of the permittivity obtained from eq. 2 are presented. They were calculated using five measurements of capacities in 5 specimens. The value of permittivity, ε_r, for the neat PVDF was lower to that given by other authors in the range from 6 to 10 [8, 9]. A possible explanation of this apparent discrepancy may come from the consideration that the SBS films are actually porous materials and therefore a contribution of the air within the pores should also account to the polarization phenomena. Considering a simple model based on the rule of mixtures, the permittivity might be expressed by the equation 6:

$$\varepsilon_r = \phi_{air} \cdot \varepsilon_{air} + \phi_m \cdot \varepsilon_m \qquad (6)$$

where ε_r, ε_{air}, ε_m are the permittivities of the solution blow spun material, air and bulk material respectively while, ϕ_{air} and ϕ_m are the volume fractions of the air and the PVDF based material in the SBS material. Taking the value of 1 for the electrical permittivity of the air, and values from 6 to 10 [8, 9] for the permittivity of the PVDF, an estimation of the volume fraction of air contained in the SBS PVDF can be obtained.

$$\phi_{air} = \frac{\varepsilon_m - \varepsilon_r}{\varepsilon_m - \varepsilon_{air}} \qquad (7)$$

Making calculations, the estimated volume fraction of air in the SBS PVDF would be within the range 0.7 – 0.8.

Table 3 Mean values of the permittivity obtained using eq. 2.

Sample	ε_r
PVDF-0%	3.0 ± 0.2
PVDF-0.5%	4.9 ± 0.4
PVDF-1.0%	3.3 ± 0.2
PVDF-2.0%	117 ± 33
PVDF-3.0%	590 ± 25
PVDF-5.0%	672 ± 33

Another way of estimating the volume fraction of air might be by the use of gravimetry. The volume of the specimens, V_T, is calculated using their accurately measured dimensions. Then, the specimens are weighted in a microbalance and by using the PVDF density the real volume of the PVDF can be obtained, VPVDF=mass/density. Finally, the volume of air within the pores of the specimens can be obtained by subtraction, $V_{air} = V_T - V_{PVDF}$ and therefore the volume fraction of air, $\phi_{air}=V_{air}/V_T$. Using the gravimetric method the volume fraction of air obtained for the SBS neat PVDF was 0.63, which is nearly in accordance with that estimated from the capacity measurements.

Finally, in order to better visualize the electrical effect of the presence of MWCNT in the PVDF polymer a plot of the permittivity as a function of the nanotubes content is shown in Fig. 13. It can be observed how the permittivity slightly increases at low concentrations of MWCNT up to about 1% by weight. Then, there is an abrupt increase and, at a weight fraction of about 3%, the permittivity starts levelling off. This behaviour points out the existence of a clear transition (electrical percolation) in the system from a dielectric to a conductive material. Designing materials trying to control the point at which this transition occurs is more than essential since it would be possible to prepare a material from one having a relatively low dielectric constant to other with a conductivity that might even be modulated depending on the temperature (piroelectricity).

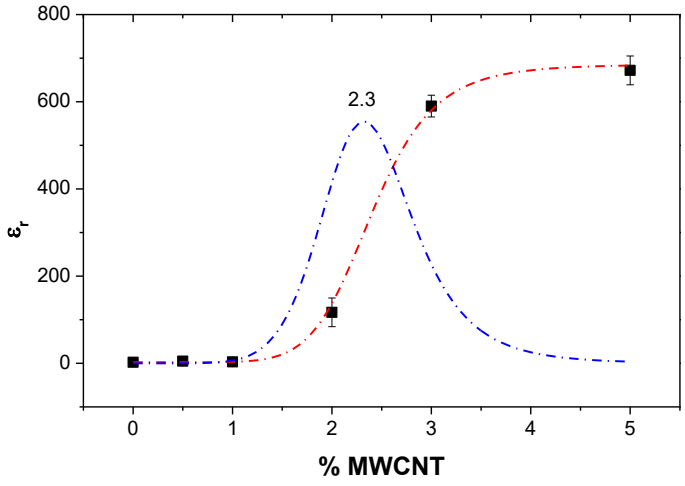

Fig. 13 Electrical permittivity for the SBS system PVDF/MWCNT as a function of the MWCNT content.

In order to estimate the percolation composition in the system PVDF/MWCNT the data of Fig. 13 were fitted using a logistic function (red dashed-dot line) to subsequently obtain its derivative which maximum pointed out the value of the percolation fraction in weight percent, ϕ_{pf}=2.3 %, for the SBS PVDF/MWCNT system. This value of percolation is close to those that can be found in the literature from 1.2 wt% to 2.5 w% [20, 60, 61].

4. Conclusions

Solution blow spinning, SBS, was used to prepared nanocomposites based on poly(vinylidene fluoride), PVDF, filled with multiwalled carbon nanotubes, MWCNT. Mats constituted by submicrometric fibers with MWCNT uniformly dispersed and well aligned along the PVDF fibers were obtained. Although the amount of MWCNT nanofiller did not affect much the fibrous morphology of the materials, slight effect on the surface roughness and consequently on the hydrophobicity occurred. It was observed that SBS used to prepare the system PVDF/MWCNT, at least under the processing conditions used, lead to materials for which the PVDF only crystallized in the β and γ phases, being the former increased with the MWCNT content. On the other hand, complementary studies by FTIR and DSC evidenced that, higher melting temperatures of the PVDF does not necessarily mean higher content of β phase as several authors have stated. Finally, the representation of electrical permittivity as a function of MWCNT content allowed obtaining a value of the percolation fraction of ϕ_{pf}=2.3% (weight percent). The main consequence of the information obtained is the possibility of designing porous reinforced PVDF materials, preferentially crystallized in the most electroactive phases, having under control the point at which the electrical percolation occurs. Thus, there exists the possibility of tailoring novel piezoelectric materials for which conductivity might be tuned depending on temperature (piroelectricity).

Disclosure of potential conflicts of interest

Funding: This study was funded by the Ministerio de Economía y Competitividad [MAT2014-59116-C2].
Conflict of Interest: The authors declare that they have no conflict of interest.

5. References

1. Dang ZM, Shen Y, Nan CW (2003) Dielectric behavior of three-phase percolative Ni-BaTiO3/polyvinylidene fluoride composites. Appl Phys Lett 81:4814–4816. https://doi.org/10.1063/1.1529085
2. Dang ZM, Fan LZ, Shen Y, Nan CW (2003) Study on dielectric behavior of a three-phase CF(PVDF + BaTiO3) composite. Chem Phys Lett 369:95–100. https://doi.org/10.1016/S0009-2614(02)01992-9
3. Yao S-H, Dang Z-M, Jiang M-J, Bai J (2008) BaTiO[sub 3]-carbon nanotube/polyvinylidene fluoride three-phase composites with high dielectric constant and low dielectric loss. Appl Phys Lett 93:182905. https://doi.org/10.1063/1.3013833
4. Dang ZM, Yuan JK, Zha JW, et al (2012) Fundamentals, processes and applications of high-permittivity polymer-matrix composites. Prog. Mater. Sci. 57:660–723
5. Choi HW, Heo YW, Lee JH, et al (2006) Effects of BaTiO3 on dielectric behavior of BaTiO 3-Ni-polymethyl methacrylate composites. Appl Phys Lett 89:. https://doi.org/10.1063/1.2354425
6. Zhou Y, Bai Y, Yu K, et al (2013) Excellent thermal conductivity and dielectric properties of polyimide composites filled with silica coated self-passivated aluminum fibers and nanoparticles. Appl Phys Lett 102:252903. https://doi.org/10.1063/1.4812653

7. Da Silva AB, Arjmand M, Sundararaj U, Bretas RES (2014) Novel composites of copper nanowire/PVDF with superior dielectric properties. Polym (United Kingdom) 55:226–234. https://doi.org/10.1016/j.polymer.2013.11.045
8. Lau KT, Hui D (2002) The revolutionary creation of new advanced materials—carbon nanotube composites. Compos Part B Eng 33:263–277. https://doi.org/10.1016/S1359-8368(02)00012-4
9. Sanchez FA, González-Benito J (2017) PVDFBaTiO 3 /carbon nanotubes ternary nanocomposites: Effect of nanofillers and processing. Polym Compos 38:227–235. https://doi.org/10.1002/pc.23579
10. Lee JS, Kim GH, Kim WN, et al (2008) Crystal Structure and Ferroelectric Properties of Poly(vinylidene fluoride)-Carbon nano tube Nanocomposite Film. Mol Cryst Liq Cryst 491:247–254. https://doi.org/10.1080/15421400802330861
11. Yan J, Liu M, Jeong YG, et al (2018) Performance Enhancements in Poly(vinylidene fluoride)-based Piezoelectric Nanogenerators for Efficient Energy Harvesting. Nano Energy 56:662–692. https://doi.org/10.1016/j.nanoen.2018.12.010
12. Chen QX, Payne P a (1995) Industrial applications of piezoelectric polymer transducers. Meas Sci Technol 6:249–267. https://doi.org/10.1088/0957-0233/6/3/001
13. Gregorio R, Capitão RC (2000) Morphology and phase transition of high melt temperature crystallized poly(vinylidene fluoride). J Mater Sci 35:299–306. https://doi.org/10.1023/A:1004737000016
14. Gregorio R, Borges DS (2008) Effect of crystallization rate on the formation of the polymorphs of solution cast poly(vinylidene fluoride). Polymer (Guildf) 49:4009–4016. https://doi.org/10.1016/j.polymer.2008.07.010
15. Olmos D, Montero F, González-Gaitano G, González-Benito J (2013) Structure and morphology of composites based on polyvinylidene fluoride filled with BaTiO 3 submicrometer particles: Effect of processing and filler content. Polym Compos 34:2094–2104. https://doi.org/10.1002/pc.22618
16. Nunes JS, Wu A, Gomes J, et al (2009) Relationship between the microstructure and the microscopic piezoelectric response of the alpha- and beta-phases of poly(vinylidene fluoride). Appl Phys a-Materials Sci Process 95:875–880. https://doi.org/DOI 10.1007/s00339-009-5089-2
17. Gomes J, Serrado Nunes J, Sencadas V, Lanceros-Mendez S (2010) Influence of the β-phase content and degree of crystallinity on the piezo- and ferroelectric properties of poly(vinylidene fluoride). Smart Mater Struct 19:065010. https://doi.org/10.1088/0964-1726/19/6/065010
18. Yue XU, Wei-tao Z, Wen-xue YU, et al (2009) Crystallization Behavior and Mechanical Properties of Poly (vinylidene fluoride)/ multi-walled Carbon Nanotube Nanocomposites. Chem Res Chinese Univ 26:491–495
19. Tang XG, Hou M, Zou J, et al (2012) Toughening and reinforcement of poly(vinylidene fluoride) nanocomposites with " bud-branched" nanotubes. Compos Sci Technol 72:263–268. https://doi.org/10.1016/j.compscitech.2011.11.011
20. Hong SM, Hwang SS (2008) Physical Properties of Thin PVDF/MWNT (Multi-Walled Carbon Nanotube) Composite Films by Melt Blending. J Nanosci Nanotechnol 8:4860–4863. https://doi.org/DOI 10.1166/jnn.2008.IC49
21. Sencadas V, Gregorio R, Lanceros-Mendez S (2009) α to β Phase Transformation and Microestructural Changes of PVDF Films Induced by Uniaxial Stretch. J Macromol Sci Part B 48:514–525.

https://doi.org/10.1080/00222340902837527
22. Mohammadi B, Yousefi AA, Bellah SM (2007) Effect of tensile strain rate and elongation on crystalline structure and piezoelectric properties of PVDF thin films. Polym Test 26:42–50. https://doi.org/10.1016/j.polymertesting.2006.08.003
23. Lee SH, Cho HH (2010) Crystal structure and thermal properties of poly(vinylidene fluoride)-carbon fiber composite films with various drawing temperatures and speeds. Fibers Polym 11:1146–1151. https://doi.org/10.1007/s12221-010-1146-x
24. Olmos D, Domínguez C, Castrillo PD, Gonzalez-Benito J (2009) Crystallization and final morphology of HDPE: Effect of the high energy ball milling and the presence of TiO2 nanoparticles. Polymer (Guildf) 50:1732–1742. https://doi.org/10.1016/j.polymer.2009.02.011
25. Sánchez F a., Redondo M, González-Benito J (2015) Influence of BaTiO\n3\n submicrometric particles on the structure, morphology, and crystallization behavior of poly(vinylidene fluoride). J Appl Polym Sci 132:n/a-n/a. https://doi.org/10.1002/app.41497
26. Chen E-C, Wu T-M (2007) Isothermal crystallization kinetics and thermal behavior of poly(ε-caprolactone)/multi-walled carbon nanotube composites. Polym Degrad Stab 92:1009–1015. https://doi.org/10.1016/j.polymdegradstab.2007.02.019
27. Feng J, Sui J, Cai W, et al (2008) Preparation and characterization of magnetic multi-walled carbon nanotubes-poly(l-lactide) composite. Mater Sci Eng B Solid-State Mater Adv Technol 150:208–212. https://doi.org/10.1016/j.mseb.2008.05.017
28. Linghao He, Qun Xu, Chengwu Hua RS (2010) Effect of Multi-Walled Carbon Nanotubes on Crystallization, Thermal, and Mechanical Properties of Poly(vinylidene fluoride. Polym Compos 16:921–927. https://doi.org/10.1002/pc
29. Linghao He, Jing Sun, Xiaoli Zheng, Qun Xu RS (2010) Effect of Multiwalled Carbon Nanotubes on Crystallization Behavior of Poly(vinylidene fluoride) in Different Solvents. Polym Polym Compos 21:449–456. https://doi.org/10.1002/app
30. He L, Zheng X, Xu Q (2010) Modification of carbon nanotubes using poly(vinylidene fluoride) with assistance of supercritical carbon dioxide: the impact of solvent. J Phys Chem B 114:5257–62. https://doi.org/10.1021/jp911621y
31. Doshi J, Reneker DH (1993) Electrospinning process and applications of electrospun fibers. Conf Rec 1993 IEEE Ind Appl Conf Twenty-Eighth IAS Annu Meet 35:151–160. https://doi.org/10.1109/IAS.1993.299067
32. Eliton S. Medeiros, Gregory M. Glenn Artur P. Klamczynski, William J. Orts LHCM (2009) Solution Blow Spinning: A New Method to Produce Micro- and Nanofibers from Polymer Solutions. J Appl Polym Sci 113:2322–2330. https://doi.org/DOI 10.1002/app.30275
33. González-Benito J, Teno J, González-Gaitano G, et al (2017) PVDF/TiO2 nanocomposites prepared by solution blow spinning: Surface properties and their relation with S. Mutans adhesion. Polym Test 58:21–30. https://doi.org/10.1016/j.polymertesting.2016.12.005
34. Kedem S, Schmidt J, Paz Y, Cohen Y (2005) Composite polymer nanofibers with carbon nanotubes and titanium dioxide particles. Langmuir 21:5600–4. https://doi.org/10.1021/la0502443

35. Huang S, Aik Yee W, Chauhari Tiju W, et al (2008) Electrospinning of PVDF with CNT : synergistic effects of extensional force and interfacial interaction on crystalline structure. Langmuir 24:13621–13626
36. Wu C-M, Chou M-H, Zeng W-Y (2018) Piezoelectric Response of Aligned Electrospun Polyvinylidene Fluoride/Carbon Nanotube Nanofibrous Membranes. Nanomaterials 8:420. https://doi.org/10.3390/nano8060420
37. Abdal-Hay A, Hamdy AS, Abdellah MY, Lim J (2014) In vitro bioactivity of implantable Ti materials coated with PVAc membrane layer. Mater Lett 126:267–270. https://doi.org/10.1016/j.matlet.2014.04.048
38. Abdal-Hay A, Vanegas P, Lim JK (2014) Air jet spray of nylon 6 membrane structures for bone tissue engineering. Mater Lett 125:51–55. https://doi.org/10.1016/j.matlet.2014.03.138
39. Kuk E, Ha YM, Yu J, et al (2016) Robust and Flexible Polyurethane Composite Nanofibers Incorporating Multi-Walled Carbon Nanotubes Produced by Solution Blow Spinning. Macromol Mater Eng 301:364–370. https://doi.org/10.1002/mame.201500298
40. Medeiros ES, Glenn GM, Klamczynski AP, et al (2014) Solution Blow Spinning. 1
41. Rosenberg Y, Siegmann A, Narkis M, Shkolnik S (1991) The sol/gel contribution to the behavior of γ-irradiated poly(vinylidene fluoride). J Appl Polym Sci 43:535–541. https://doi.org/10.1002/app.1991.070430314
42. Seoul C, Kim YT, Baek CK (2003) Electrospinning of poly(vinylidene fluoride)/dimethylformamide solutions with carbon nanotubes. J Polym Sci Part B Polym Phys 41:1572–1577. https://doi.org/10.1002/polb.10511
43. Cai X, Lei T, Sun D, Lin L (2017) A critical analysis of the α, β and γ phases in poly(vinylidene fluoride) using FTIR. RSC Adv 7:15382–15389. https://doi.org/10.1039/C7RA01267E
44. González-Benito J, González-Gaitano G (2008) Interfacial conformations and molecular structure of PMMA in PMMA/silica nanocomposites. Effect of high-energy ball milling. Macromolecules 41:4777–4785. https://doi.org/10.1021/ma800260k
45. Olmos D, Martín E V., González-Benito J (2014) New molecular-scale information on polystyrene dynamics in PS and PS–BaTiO3 composites from FTIR spectroscopy. Phys Chem Chem Phys 16:24339–24349. https://doi.org/10.1039/C4CP03516J
46. Priya L, Jog JP (2002) Poly(vinylidene fluoride)/clay nanocomposites prepared by melt intercalation: Crystallization and dynamic mechanical behavior studies. J Polym Sci Part B Polym Phys 40:1682–1689. https://doi.org/10.1002/polb.10223
47. Manna S, Nandi AK (2007) Piezoelectric β polymorph in poly(vinylidene fluoride)-functionalized multiwalled carbon nanotube nanocomposite films. J Phys Chem C 111:14670–14680. https://doi.org/10.1021/jp073102l
48. Mandal A, Nandi AK (2011) Physical properties of poly(vinylidene fluoride) composites with polymer functionalized multiwalled carbon nanotubes using nitrene chemistry. J Mater Chem 21:15752. https://doi.org/10.1039/c1jm12926k
49. Kar E, Bose N, Dutta B, et al (2017) Poly(vinylidene fluoride)/submicron graphite platelet compositeA smart, lightweight flexible material with significantly enhanced β polymorphism, dielectric and microwave shielding properties. Eur Polym J 90:442–455. https://doi.org/10.1016/j.eurpolymj.2017.03.030
50. Jia N, He Q, Sun J, et al (2017) Crystallization behavior and electroactive

properties of PVDF, P(VDF-TrFE) and their blend films. Polym Test 57:302–306. https://doi.org/10.1016/j.polymertesting.2016.12.003
51. Tsonos C, Pandis C, Soin N, et al (2015) Multifunctional nanocomposites of poly(vinylidene fluoride) reinforced by carbon nanotubes and magnetite nanoparticles. Express Polym Lett 9:1104–1118. https://doi.org/10.3144/expresspolymlett.2015.99
52. Marega C, Marigo A (2003) Influence of annealing and chain defects on the melting behaviour of poly(vinylidene fluoride). Eur Polym J 39:1713–1720. https://doi.org/10.1016/S0014-3057(03)00062-4
53. Chiu FC (2014) Comparisons of phase morphology and physical properties of PVDF nanocomposites filled with organoclay and/or multi-walled carbon nanotubes. Mater Chem Phys 143:681–692. https://doi.org/10.1016/j.matchemphys.2013.09.054
54. Chiu FC, Chen YJ (2015) Evaluation of thermal, mechanical, and electrical properties of PVDF/GNP binary and PVDF/PMMA/GNP ternary nanocomposites. Compos Part A Appl Sci Manuf 68:62–71. https://doi.org/10.1016/j.compositesa.2014.09.019
55. Ramasundaram S, Yoon S, Kim KJ, Park C (2008) Preferential formation of electroactive crystalline phases in poly(vinylidene fluoride)/organically modified silicate nanocomposites. J Polym Sci Part B Polym Phys 46:2173–2187. https://doi.org/10.1002/polb.21550
56. Gregorio, R, Cestari M (1994) Effect of crystallization temperature on the crystalline phase content and morphology of poly(vinylidene fluoride). J Polym Sci Part B Polym Phys 32:859–870. https://doi.org/10.1002/polb.1994.090320509
57. Gregorio R (2006) Determination of the α, β, and γ crystalline phases of poly(vinylidene fluoride) films prepared at different conditions. J Appl Polym Sci 100:3272–3279. https://doi.org/10.1002/app.23137
58. Ince-Gunduz BS, Alpern R, Amare D, et al (2010) Impact of nanosilicates on poly(vinylidene fluoride) crystal polymorphism: Part 1. Melt-crystallization at high supercooling. Polymer (Guildf) 51:1485–1493. https://doi.org/10.1016/j.polymer.2010.01.011
59. Biswas S, Dutta B, Bhattacharya S (2017) Isothermal crystallization kinetics as a probe of the preferential electroactive phase nucleation in silver-poly(vinylidene fluoride) nanocomposites: Dependence on nanoparticle size and concentration. Eur Polym J 86:1–16. https://doi.org/10.1016/j.eurpolymj.2016.11.013
60. Li L, Zhang M, Ruan W (2015) Studies on synergistic effect of CNT and CB nanoparticles on PVDF. Polym Compos 36:2248–2254. https://doi.org/10.1002/pc.23137
61. Wang L, Dang Z-M (2005) Carbon nanotube composites with high dielectric constant at low percolation threshold. Appl Phys Lett 87:042903. https://doi.org/10.1063/1.1996842